Effect of CeF_3 Addition on the Nucleation and Up-Conversion Luminescence in Transparent Oxyfluoride Glass−Ceramics

G. Dantelle,[†] M. Mortier,*[,†] D. Vivien,[†] and G. Patriarche[‡]

Laboratoire de Chimie Appliquée de l'Etat Solide, CNRS-UMR 7574, ENSCP-11, rue Curie, 75005 Paris, France, and Laboratoire de Photonique et Nanostructures, CNRS-UPR20, route de Nozay, 91460 Marcoussis.

Received December 14, 2004. Revised Manuscript Received February 2, 2005

GeO_2:PbO:PbF_2 glasses doped with ErF_3, YbF_3, and CeF_3 were successfully synthesized. Highly transparent doped glass−ceramics were prepared by annealing the glasses at 360 °C, leading to nanocomposites made of β-PbF_2 crystallites embedded into an amorphous oxide phase. The effect of CeF_3 on the nucleation process was studied, revealing that CeF_3, as ErF_3 and YbF_3, acts as seeds for β-PbF_2 heterogeneous nucleation, but with higher nucleation efficiency. Transmission electron microscopy indicates that spherical 8-nm crystallites are formed. Energy dispersive X-ray microanalysis tends to indicate that fluoride crystallites contained high concentrations of rare-earth ions, forming a solid solution $Pb_{1-x-y-z}Er_xYb_yCe_zF_{2+x+y+z}$, which has been confirmed by a study of the crystallites unit cell parameter. The optical properties of the tri-doped glass−ceramics were compared to those of Yb:Er-codoped glass−ceramics. The influence of CeF_3 on the Er^{3+} emission and on the fluorescence decay curve of the $^4I_{13/2}$ emitting level of Er^{3+} was studied. In glass−ceramics containing CeF_3, Er^{3+} up-conversion fluorescence nearly vanishes at the benefit of the 1.54-μm Er^{3+} fluorescence which is enhanced.

Introduction

For several years, transparent glass−ceramics have been investigated as hosts for rare-earth ions to obtain materials that are easy to shape and with high performances for optical applications.[1] Glass−ceramics are usually obtained by glasses annealing, leading to the partial crystallization of the materials. When the dispersed crystalline phase is of small size compared to the light wavelengths, glass−ceramics are transparent.

Among the studied glass−ceramics, the transparent oxyfluoride type ,[2,3] composed of an amorphous oxide phase with nanosized fluoride crystallites embedded into it, are of great interest. Glass−ceramics codoped with ErF_3 and YbF_3 (SiO_2:Al_2O_3:PbF_2:CdF_2+ErF_3+YbF_3) were first described by Wang and Ohwaki[2] as materials for Er^{3+} green up-conversion emission. We have recently investigated GeO_2:PbO:PbF_2 glass−ceramics codoped with ErF_3 and YbF_3.[4] The thermal behavior and morphology of these codoped glass−ceramics were studied, revealing that the fluoride phase (β-PbF_2) nucleation was initiated by the rare-earth fluorides. It has been demonstrated that both ErF_3 and YbF_3 act as nucleating agent but that ErF_3 has the highest nucleation efficiency and governs the nucleation process in Yb:Er-codoped samples.

In oxyfluoride glass−ceramics, because rare-earth ions are mostly segregated inside the crystallites[5−7] they are lying in a fluoride crystalline environment with large optical band gap and low phonon energy and consequently possess appropriate properties for optical applications.[8] The 1.54-μm emission is particularly interesting as it can be used in eye-safe range-finding and optical fibers telecommunications. To achieve such emission, Er^{3+} ions are used as doping ions because of their $^4I_{13/2} \rightarrow {}^4I_{15/2}$ transition. Nonetheless, Yb^{3+} ions are usually added as sensitizer, enabling a higher pumping rate at 980 nm using commercially available laser diodes. Thus, glass−ceramics codoped with Er^{3+} and Yb^{3+} ions are required.

To enhance the 1.54-μm emission intensity, trivalent cerium ions have been added to Yb:Er-codoped crystals[9] or in glasses.[10] In particular, in the Yb:Er:$Ca_2Al_2SiO_7$ crystal, laser properties were strongly improved by the introduction of Ce^{3+} ions.[11] Indeed, the addition of Ce^{3+} ions enabled increase of the laser slope efficiency by a factor of 2 and the laser threshold became about five times smaller,[11] thanks to the reduction of up-conversion losses. Hence, from the optics viewpoint, three doping ions (Er^{3+}, Yb^{3+}, Ce^{3+}) may be interesting in glass−ceramics too, to promote the 1.54-

* Corresponding author. E-mail: michel-mortier@enscp.fr. Tel: 33 1 53 73 79 27. Fax: 33 1 46 34 74 89.
[†] Laboratoire de Chimie Appliquée de l'Etat Solide.
[‡] Laboratoire de Photonique et Nanostructures.

(1) Dejneka, M. J. *MRS Bull.* **1998**, *23* (11), 57.
(2) Wang, Y.; Ohwaki, J. *Appl. Phys. Lett.* **1993**, *63* (24), 3268.
(3) Mortier, M.; Goldner, P.; Chateau, C.; Genotelle, M. *J. Alloys Compd.* **2001**, *323*−*324*, 245.
(4) Dantelle, G.; Mortier, M.; Vivien, D.; Patriarche, G. *J. Mater. Res.* **2005**, *20* (2), 472.
(5) Mortier, M.; Auzel, F. *J. Non-Cryst. Solids* **1999**, *256&257*, 361.
(6) Tick, P. A.; Borrelli, N. F.; Cornelius, L. K.; Newhouse, M. A. *J. Appl. Phys.* **1995**, *78* (11), 6367.
(7) Abril, M.; Mendez-Ramos, J.; Martin, I. R.; Rodriguez-Mendoza, U. R.; Lavin, V.; Delgado-Torres, A.; Rodriguez, V. D. *J. Appl. Phys.* **2004**, *95* (10), 5271.
(8) Mortier, M. *Philos. Mag. B* **2002**, *82* (6), 745.
(9) Simondi-Tessaire, B.; Viana, B.; Vivien, D.; Lejus, A. M. *Opt. Mater.* **1996**, *6* 267.
(10) Yang, J.; Zhang, L.; Wen, L.; Dai, S.; Hu, L.; Jiang, Z. *Chem. Phys. Lett.* **2004**, *384*, 295.
(11) Simondi-Tesseire, B.; Viana, B.; Lejus, A. M.; Benitez, J. M.; Vivien, D.; Borel, C.; Templier, R.; Wyon, C. *IEEE J. Quantum Electron.* **1996**, *32* (11), 2004.

10.1021/cm047821d CCC: $30.25
Published on Web 03/25/2005

μm Er^{3+} emission instead of Er^{3+} visible up-conversion emission.[2]

In this paper we will discuss the influence of CeF_3 addition on Yb:Er-codoped GeO_2:PbO:PbF_2 glass−ceramics. At first, we will report the successful preparation of glasses doped with ErF_3, YbF_3, and CeF_3, which lead to transparent oxyfluoride tri-doped glass−ceramics after an appropriate heat treatment. We will study the nucleation efficiency of CeF_3 compared to the one of ErF_3 and YbF_3 and we will describe the morphology of the nanocrystallites in those tri-doped glass−ceramics. Second, we will highlight the advantages of CeF_3 addition on the optical properties of Yb:Er-codoped glass−ceramics. We especially studied the Er^{3+} green up-conversion emission, the fluorescence decay profiles of the $^4S_{3/2}$, $^4I_{11/2}$, and $^4I_{13/2}$ levels of Er^{3+}, and the Er^{3+} 1.54 μm-fluorescence.

Experimental Section

A. Preparation. The samples investigated in the present study possess the following composition: 50:40:10 GeO_2/PbO/PbF_2, rare-earth fluorides being added in excess. Hereafter 50:40:10 GeO_2/PbO/PbF_2 will be labeled GPF.

A series of glasses doped with ErF_3, YbF_3, and CeF_3 (tri-doped glasses) was prepared with the following composition: GPF + $0.5ErF_3$ + $1YbF_3$ + $zCeF_3$, z = [0; 0.2; 0.4; 0.5; 0.6] (mol %). Two other samples codoped with ErF_3 and YbF_3 were also prepared for comparison: GPF + $1ErF_3$ + $1YbF_3$ and GPF + $0.5ErF_3$ + $1.5YbF_3$.

Crystalline powders of GeO_2 (purity: 99.999%), PbO (purity: 99%), and PbF_2 (purity: 99.997%) were mixed together in an agate mortar. Then, the 4N-purity fluorides ErF_3, YbF_3, and CeF_3 were added. The mixture was placed into a platinum crucible and heated at 1050 °C in air for 20 min. Then, the molten glasses were poured between two copper plates, previously heated at ∼150 °C to limit thermal shocks. To reduce internal strains, the obtained glasses were annealed for 2 h at 50 °C below their vitreous transition temperature as measured by differential thermal analysis (DTA).

B. Measurements. Glasses were investigated by DTA in a double symmetric analyzer (TAG24 Setaram). The samples were ground and sifted to obtain particles with a size between 45 and 71 μm. For the measurements, the powder samples were compared to burnt alumina, a neutral component in the temperature range explored. The DTA measurements were performed under argon atmosphere. At a heating rate of 10 °C per minute, the temperature was increased from 30 to 850 °C, which corresponds to the temperature range where the vitreous transition, crystallizations, and fusions occur. All temperatures reported hereafter were taken at the maximum of the peaks.

X-ray diffraction (XRD) measurements were performed on a Siemens D5000 diffractometer using a Co anode ($\lambda_{K\alpha 1}$ = 1.789 Å) with a resolution of $2\theta = 0.05°$. The 2θ interval was taken between 25° and 65° with 0.02° increments. The XRD diagram is made of thin peaks superimposed to a broad diffuse background corresponding to the glassy matrix. The crystallites size was calculated using the Scherrer formula. An XRD ratio, R, roughly evaluating the amount of crystalline phase in the glass−ceramics, was calculated with the following expression:

$$R = \frac{\textit{Area of the crystalline peaks}}{\textit{Total area of the XRD diagram}}$$

with the total area corresponding to the diagram integration from 2θ = 25−65°.

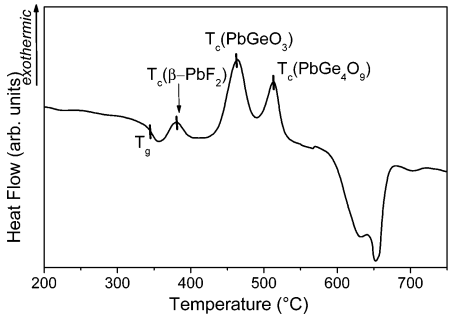

Figure 1. DTA curve of the GPF + $0.5ErF_3$ + $1YbF_3$ + $0.5CeF_3$ glass.

Transmission electron microscopy (TEM) was performed on a 200-kV Philips CM20 microscope. The samples were ground into very fine powder that was placed onto a carbon-coated copper grid and introduced into the microscope. TEM images and the associated selected area electron diffraction (SAED) patterns were studied, enabling the description of the glass−ceramics morphology. High-resolution TEM (HRTEM) images were taken to observe atomic planes inside the crystallites. The microscope was equipped with an energy dispersive X-ray (EDX) analyzer which enables glass−ceramics microanalysis.

Emission spectra in the visible range were recorded under 8-ns pulsed excitation using a tunable optical parametric oscillator (OPO), pumped by the third harmonic of a Q-switched Nd^{3+}:YAG laser (355 nm). The fluorescence was analyzed through a 250-mm monochromator equipped with an optical multichannel analyzer with a resolution better than 1.5 nm. Emission spectra in the infrared range were recorded under a CW excitation with a titanium−sapphire laser, pumped by an argon ion laser. The fluorescence was analyzed through a 250-mm monochromator and then detected by a liquid nitrogen cooled PbS cell. The resolution was better than 1.5 nm.

Fluorescence decay profiles in the infrared range and in the visible range were obtained under pulsed excitation using the OPO. The infrared fluorescence was detected by an InAs cell cooled at 77 K and connected to an oscilloscope. Appropriate band-pass filters were used to select the wavelengths of interest. The visible fluorescence was analyzed with a 250-mm monochromator and detected by the optical multichannel analyzer. The lifetimes were measured on thin powder films to avoid macroscopic reabsorption effects (radiative trapping) that could result in some artificial lengthening of the observed fluorescence decay.

Results and Discussion

A. Thermal Behavior and Morphology of Tri-Doped Glass−Ceramics. *1. Synthesis of Transparent Tri-Doped Glass−Ceramics.* The DTA curve represented in Figure 1 corresponds to the GPF-glass doped with 0.5% ErF_3, 1% YbF_3, and 0.5% CeF_3. Different thermal events such as the glass transition, crystallizations (exothermic peaks), and fusions (endothermic peaks) can be observed. The glass transition (T_g), occurring around 345 °C, is followed by three distinct crystallization peaks. The first one is centered at 380 °C and corresponds to the crystallization of a rare-earth fluoride β-PbF_2 solid solution[4] as it will be discussed later. For the sake of conciseness, this solid solution will be referred as β-PbF_2 in the following discussion. The second and third peaks correspond to the matrix crystallization. XRD experiments have highlighted the formation of two mixed oxides: $PbGeO_3$ and $PbGe_4O_9$ ($T_c(PbGeO_3)$ = 464 °C and

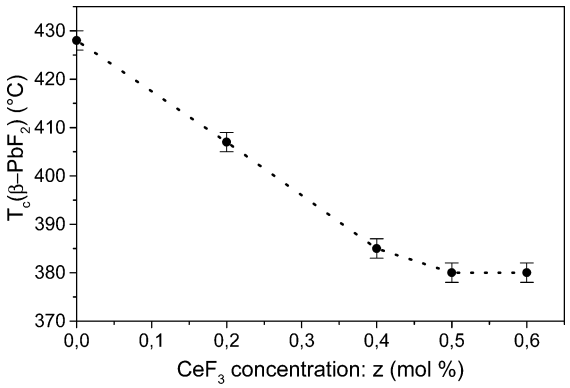

Figure 2. Evolution of β-PbF_2 crystallization temperature versus CeF_3 concentration (z) for GPF + 0.5ErF_3 + 1YbF_3 + $z$$CeF_3$ glasses.

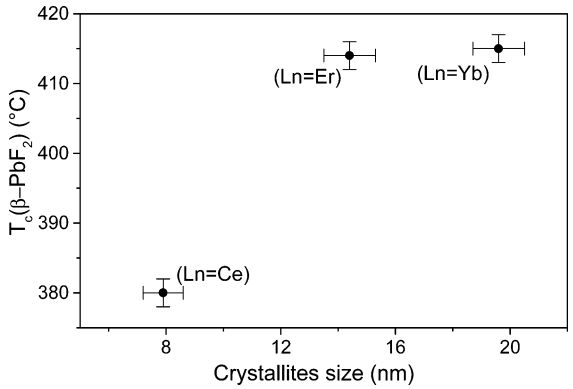

Figure 3. Evolution of β-PbF_2 crystallization temperature and of the crystallites size according to the doping nature, for the following composition: GPF + 0.5ErF_3 + 1YbF_3 + 0.5LnF_3 (Ln = Ce,Er,Yb).

$T_c(PbGe_4O_9)$ = 514 °C). The fusion of these phases, corresponding to the endothermic broad peak, is lying in the 600−675 °C temperature range.

One can notice that the β-PbF_2 crystallization peak occurs at lower temperature and is well separated from the crystallization of mixed oxides. This means that, with a well-adapted heat treatment, the partial devitrification leading to β-PbF_2 crystallites embedded into the oxide glassy phase is possible. Indeed, tri-doped glasses were devitrified by a 10-hour treatment at 360 °C, leading to transparent glass−ceramics containing β-PbF_2 crystallites.

2. Influence of CeF_3 Addition on Thermal Events. A series of tri-doped glasses with various concentrations in CeF_3 but constant concentrations in ErF_3 and YbF_3 (GPF + 0.5ErF_3 + 1YbF_3 + $z$$CeF_3$, z = [0; 0.2; 0.4; 0.5; 0.6]) was prepared. The DTA curves indicate that the position of β-PbF_2 crystallization peak varies, whereas the mixed oxides crystallization peaks and the fusion peak remain unchanged. β-PbF_2 crystallization temperature is plotted versus CeF_3 content on Figure 2 . When z = 0, $T_c(\beta\text{-}PbF_2)$ = 428 °C and when z = 0.6, $T_c(\beta\text{-}PbF_2)$ = 380 °C. For a constant erbium and ytterbium fluorides content, β-PbF_2 crystallization temperature decreases with the increase of cerium fluoride. Thus, the addition of CeF_3 strongly promotes β-PbF_2 crystallization. As already demonstrated with erbium or ytterbium fluorides,[4,5] cerium fluoride acts as seeds for the heterogeneous nucleation of β-PbF_2.

3. Nucleation Efficiency of CeF_3. The nucleation efficiency of CeF_3 was compared to those of ErF_3 and YbF_3. The following glasses were studied: GPF + 0.5ErF_3 + 1YbF_3 + 0.5LnF_3 (where Ln = Er, Yb, or Ce). The starting glasses contained 0.5% ErF_3 and 1% YbF_3, and in addition, a small amount of rare-earth fluorides (either 0.5% ErF_3 or 0.5% YbF_3 or 0.5% CeF_3) was introduced. The glasses were analyzed by DTA and, after a devitrification treatment, the obtained glass−ceramics were analyzed by XRD. On Figure 3, β-PbF_2 crystallization temperatures, obtained by DTA, and crystallites sizes, evaluated by fitting the X-ray diffraction peaks with a Gaussian line and using the Scherrer formula, are reported according to the additional doping fluoride.

When LnF_3 = CeF_3, $T_c(\beta\text{-}PbF_2)$ = 380 °C, whereas when the additional doping is ErF_3 or YbF_3, β-PbF_2 crystallizes at higher temperature (414 and 415 °C, respectively). The addition of CeF_3 strongly enhances β-PbF_2 crystallization compared to the addition of ErF_3 and YbF_3. Moreover, the crystallites size varies according to the additional doping fluoride. Cerium fluoride addition leads to 8-nm crystallites whereas the addition of the two other fluorides leads to about twice larger crystallites (Figure 3). The XRD ratios R of the three samples are almost the same (R = 23% for Ln = Er, R = 22% for Ln = Yb and for Ln = Ce), meaning that in all cases nearly the same amount of β-PbF_2 has crystallized. Consequently, a decrease of the crystallites size corresponds to an increase of the seeds number. The CeF_3-rich glass−ceramic, containing the smallest crystallites, produces the largest number of nuclei, which reflects the highest efficiency of CeF_3 in promoting β-PbF_2 nucleation.

Both DTA and XRD measurements showed that CeF_3 has the highest nucleation efficiency. And, as it has been demonstrated in a previous study,[4] ErF_3 has higher nucleation efficiency than YbF_3. The high nucleation efficiency of CeF_3 can explain the problems that were encountered in such glasses synthesis. Indeed, as reported on Figure 2, above 0.5% CeF_3, $T_c(\beta\text{-}PbF_2)$ = 380 °C, what is close to the vitreous transition temperature (345 °C), leading to difficulties in maintaining the glassy state upon pouring from the melt. Above 0.6% CeF_3-doping, glasses become opaque, showing that spontaneous devitrification occurs during glass preparation.

4. Morphology of Glass−Ceramics Containing ErF_3, YbF_3 and CeF_3. TEM study of GPF + 0.5ErF_3 + 1YbF_3 + 0.5CeF_3 glass−ceramic was performed. Figure 4a presents the dark field micrograph and 4b presents the associated SAED pattern. On Figure 4a, one can observe many spherical crystallites lying on the gray background corresponding to the glassy phase. The crystallites size distribution, obtained from the analysis of the TEM image (Figure 4a), is presented in Figure 5. It shows an average crystallites size of 8 nm with a standard deviation of 1 nm, meaning that the crystallites size is very homogeneous. The TEM size evaluation is in good agreement with the XRD calculation (7.9 ± 0.5 nm) reported on Figure 3.

On the associated SAED pattern (Figure 4b), beside the large circle associated with the diffuse scattering of the glassy matrix, one can observe numerous spots, situated on virtual circles, which correspond to the different diffraction planes. This pattern looks like a polycrystalline material pattern, reflecting the independent orientation of the crystallites. Many β-PbF_2 crystallites are in diffraction conditions, but

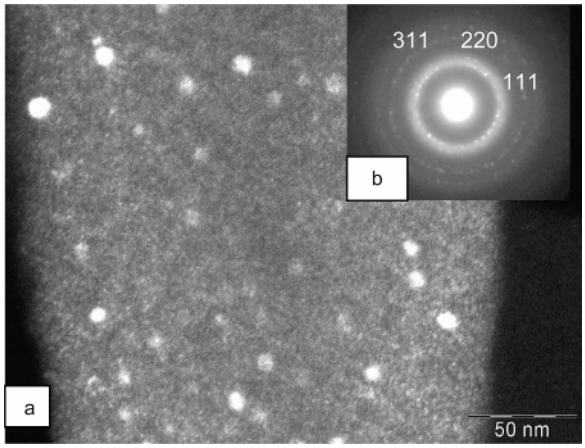

Figure 4. TEM image (a) and SAED pattern (b) of GPF + $0.5ErF_3$ + $1YbF_3$ + $0.5CeF_3$ glass−ceramic.

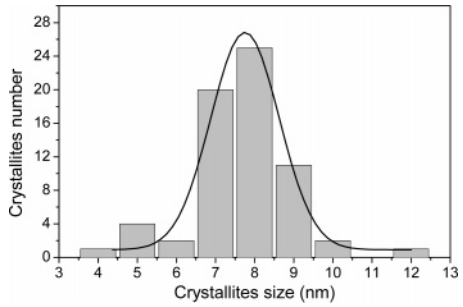

Figure 5. Crystallites size distribution in GPF + $0.5ErF_3$ + $1YbF_3$ + $0.5CeF_3$ glass−ceramic, fitted by a Gaussian line shape.

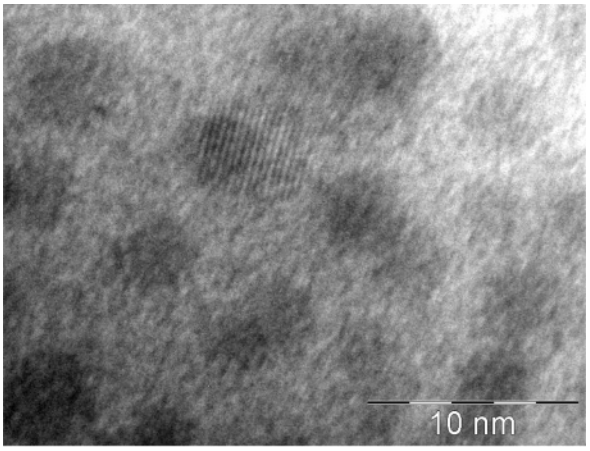

Figure 6. High-resolution TEM image of GPF + $0.5ErF_3$ + $1YbF_3$ + $0.5CeF_3$ glass−ceramic, showing the {111} atomic planes spacings.

in different crystallographic orientations, and the spots nearly form continuous circles. The spots indexation was possible by calculating the interplanar spacings *d* from the SAED pattern. The spots on the first virtual circle correspond to the diffraction of the {111} planes, followed by the {220} and the {311} planes. On the HRTEM image (Figure 6), one can clearly observe the {111} atomic planes of a crystallite. The measurement of the distance separating two planes enables reaching the interplanar distance *d*. Using the *d* values obtained either by SAED pattern analysis or by HRTEM image analysis, the unit cell parameter *a* was calculated to be $a = 5.77 \pm 0.05$ Å. This value is in good agreement with the XRD measurement $a = 5.81 \pm 0.01$ Å, deduced from the Bragg peak angular positions.

Table 1. EDX-Microanalysis of 50:40:10 GeO_2/PbO/PbF_2 + $0.5ErF_3$ + $1YbF_3$ + $0.5CeF_3$ Glass−Ceramic

element	crystalline domain (at. %)	amorphous domain (at. %)
F	16.9 ± 0.5	9.0 ± 0.5
O	40.5 ± 0.5	62.6 ± 0.5
Pb	29.1 ± 0.1	13.3 ± 0.1
Ge	9.1 ± 0.1	14.4 ± 0.1
Er	1.1 ± 0.1	0.3 ± 0.1
Yb	2.4 ± 0.1	0.4 ± 0.1
Ce	0.9 ± 0.1	0.1 ± 0.1

The unit cell parameter of the crystalline phase is much smaller than the one of pure β-PbF_2 ($a_{PbF2} = 5.94$ Å) because Pb^{2+} ions are substituted by smaller trivalent rare-earth ions into the PbF_2 crystallites, leading to the formation of a solid solution whose formula is assumed to be $Pb_{1-x-y-z}Er_xYb_y$-$Ce_zF_{2+x+y+z}$.[4,12]

5. Rare-Earth Segregation into β-PbF₂ Crystallites. EDX-microanalysis was performed to confirm the formation of such a solid solution. Nonetheless, as the crystallites size is twice smaller than the probe beam (diameter of 15 nm) and is much smaller than the analyzed sample thickness, the analyzed volume always includes both crystalline and amorphous phases. Despite this, experiments were done by successively pointing the probe beam on a crystallite, called "crystalline domain", and on a domain next to the crystallite, which we called "amorphous domain". In Table 1, the results of one representative measurement are reported.

One can obviously notice (Table 1) that, even if each domain contains crystalline phase (rich in fluorine) and amorphous phase (rich in oxygen), our denominations are relevant with the F/O proportion. In the crystalline domain, the rare-earth elements (Er, Yb, and Ce) are about five times more concentrated than in the amorphous domain. Thus, EDX-microanalysis reflects a segregation of the three rare-earth ions inside the β-PbF_2 crystallites, confirming the formation of a solid solution $Pb_{1-x-y-z}Er_xYb_yCe_zF_{2+x+y+z}$.

Furthermore, by analyzing Table 1, one can observe that Ce^{3+} ions are the most efficiently segregated into the crystallites, which is in good agreement with its higher nucleation efficiency discussed before. Moreover, it has been shown that rare-earth solubility in PbF_2 increases when the rare-earth radius increases.[13] Indeed, r_{Ce3+} (1.03 Å) is much closer to r_{Pb2+} (1.20 Å) than r_{Er3+} (0.88 Å) or r_{Yb3+} (0.86 Å). This explains why CeF_3 is more soluble in PbF_2. This could be related to the nucleation efficiency: the most soluble rare-earth fluoride is the most efficient for nucleation.

Other measurements were performed on different areas of the sample and all of them lead to analogous results.

B. Effect of CeF_3 on the Optical Properties of Yb:Er-Codoped Glass−Ceramics. *1. Up-Conversion Emission of Glass−Ceramics.* Glass−ceramics (GPF + $0.5ErF_3$ + $1YbF_3$ and GPF + $0.5ErF_3$ + $1YbF_3$ + $0.5CeF_3$) were studied in the same experimental conditions to enable a fluorescence intensity comparison. Both were excited at 920 nm, populating indirectly the $^4I_{11/2}$ level of Er^{3+} by energy transfer

(12) Tyagi, A. K.; Patwe, S. J.; Achary, S. N.; Mallia, M. B. *J. Solid State Chem.* **2004**, *177*, 1746.
(13) Dib, A.; Aléonard, S.; Roux, M. Th. *J. Solid State Chem.* **1984**, *52*, 292.

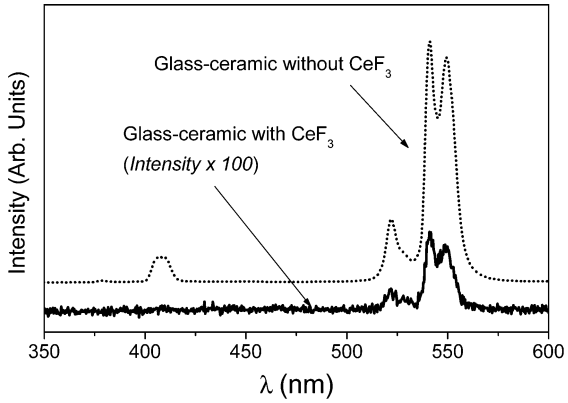

Figure 7. Up-conversion spectra of GPF + $0.5ErF_3$ + $1YbF_3$ glass−ceramic (dotted line) and GPF + $0.5ErF_3$ + $1YbF_3$ + $0.5CeF_3$ glass−ceramic (solid line). The intensity of the CeF_3-containing compound has been multiplied by 100.

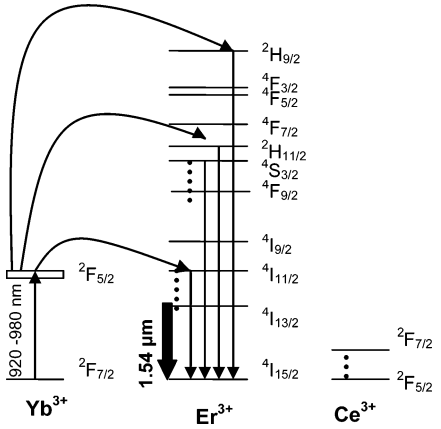

Figure 8. Energy levels diagram of Er^{3+}, Yb^{3+}, and Ce^{3+}, pointing out different energy transfer processes existing between the three ions.

through the $^2F_{5/2}$ level of Yb^{3+}. Their 1.54-μm fluorescence, corresponding to the $^4I_{13/2} \rightarrow {}^4I_{15/2}$ emission transition, was detected. In addition a green fluorescence, either strong for the GPF + $0.5ErF_3$ + $1YbF_3$ glass−ceramic or much weaker for the GPF + $0.5ErF_3$ + $1YbF_3$ + $0.5CeF_3$ glass−ceramic, can be visually observed. Thus, the spectra of these two glass−ceramics were recorded between 350 and 600 nm (Figure 7).

The GPF + $0.5ErF_3$ + $1YbF_3$ glass−ceramic spectrum is reported on Figure 7 as a dotted line. The three emission bands, observed around 540, 520, and 400 nm, arise from up-conversion fluorescence.[14] The 540- and 520-nm bands corresponding, respectively, to the $^4S_{3/2} \rightarrow {}^4I_{15/2}$ and $^2H_{11/2} \rightarrow {}^4I_{15/2}$ emission transitions of Er^{3+} are due to a two-photon process.[15] The weak emission, appearing around 400 nm, can be attributed[16] to the $^2H_{9/2} \rightarrow {}^4I_{15/2}$ emission transition, resulting from a three-photon process. All these transitions are represented on an energy levels diagram in Figure 8. As previously described by Wang and Ohwaki[2], glass−ceramics codoped with ErF_3 and YbF_3 are materials with high Er^{3+} up-conversion emission.

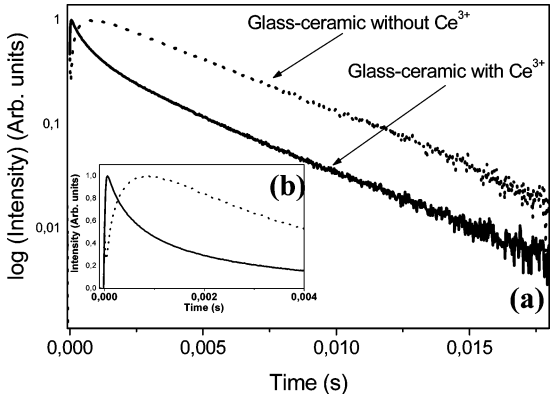

Figure 9. Fluorescence decay curves of the $^4I_{13/2}$ level of Er^{3+} emitting at 1.54 μm ($\lambda_{excitation}$ = 980 nm) for GPF + $0.5ErF_3$ + $1YbF_3$ glass−ceramic (dotted line) and for GPF + $0.5ErF_3$ + $1YbF_3$ + $0.5CeF_3$ glass−ceramic (solid line): (a) horizontal scale log(Intensity); (b) horizontal scale Intensity and focus at short time.

The up-conversion emission spectrum of the CeF_3-containing glass−ceramic, multiplied by 100, is drawn as a solid line in Figure 7. It follows that the addition of CeF_3 dramatically reduces the up-conversion emission intensity: the 520- and 540-nm emission intensities are divided by about 300, and the 400-nm emission has completely disappeared.

2. Fluorescence Decay Curves of the $^4I_{11/2}$ and $^4I_{13/2}$ levels of Er^{3+}. In two glass−ceramics (GPF + $0.5ErF_3$ + $1YbF_3$ and GPF + $0.5ErF_3$ + $1YbF_3$ + $0.5CeF_3$), the fluorescence decay curves of Er^{3+} $^4I_{11/2}$ level were recorded at 2.7 μm, corresponding to the $^4I_{11/2} \rightarrow {}^4I_{13/2}$ emission transition, under a 980-nm excitation that populated the $^4I_{11/2}$ level. The 2.7-μm fluorescence spectrum of Er^{3+}-doped glass−ceramics has already been published.[3] In the GPF + $0.5ErF_3$ + $1YbF_3$ glass−ceramic, the $^4I_{11/2}$ level lifetime τ is 590 ± 30 μs. The observation of this 2.7-μm emission is the only way to measure safely the $^4I_{11/2}$ level lifetime because of the spectral overlap between the emission arising from Yb^{3+} ions and Er^{3+} ions in the 1-μm spectral range. In the CeF_3-containing glass−ceramic, no fluorescence could be detected, indicating that the $^4I_{11/2} \rightarrow {}^4I_{13/2}$ transition is mostly nonradiative in the presence of CeF_3. CeF_3 induces nonradiative de-excitation paths between $^4I_{11/2}$ and $^4I_{13/2}$ levels.

The fluorescence decay curves of these two glass−ceramics were recorded at 1.54 μm (corresponding to the $^4I_{13/2} \rightarrow {}^4I_{15/2}$ emission transition) by exciting the samples at 1.5 μm, i.e., directly into the $^4I_{13/2}$ level. In both glass−ceramics, the $^4I_{13/2}$ level lifetime was measured: $\tau(^4I_{13/2})$ = 4.3 ± 0.2 ms in GPF + $0.5ErF_3$ + $1YbF_3$ and $\tau(^4I_{13/2})$ = 4.1 ± 0.2 ms in GPF + $0.5ErF_3$ + $1YbF_3$ + $0.5CeF_3$. These measurements indicate that CeF_3 addition does not significantly affect the Er^{3+} $^4I_{13/2}$ level lifetime.

Finally, the fluorescence decay curves of the Er^{3+} $^4I_{13/2}$ emitting level were recorded at 1.54 μm by exciting the samples at 980 nm, i.e., in the $^4I_{11/2}$ level of Er^{3+}. The fluorescence decay profiles of each glass−ceramic in logarithmic scale are reported in Figure 9a. In the glass−ceramic without CeF_3, a rise time of 360 ± 20 μs is observed (Figure 9b), meaning that the emitting level (i.e., the $^4I_{13/2}$ level) is slowly populated by the decay of the long-lived $^4I_{11/2}$ level. It should be emphasized that the $^4I_{11/2}$ fluorescence lifetime

(14) Pollnau, M.; Gamelin, D. R.; Lüthi, S. R.; Güdel, H. U. *Phys. Rev. B* **2000**, *61* (5), 3337.
(15) Mendez-Ramos, J.; Lavin, V.; Martin, I. R.; Rodriguez-Mendoza, U. R.; Gonzalez-Almeida, J. A.; Rodriguez, V. D.; Lozano-Gorrin, A. D.; Nunez, P. *J. Alloys Compd.* **2001**, *323*−*324*, 753.
(16) Gouveia-Neto, A. S.; da Costa, E. B.; Bueno L. A.; Ribeiro, S. J. L. *J. Alloys Compd.* **2004**, *375*, 224.

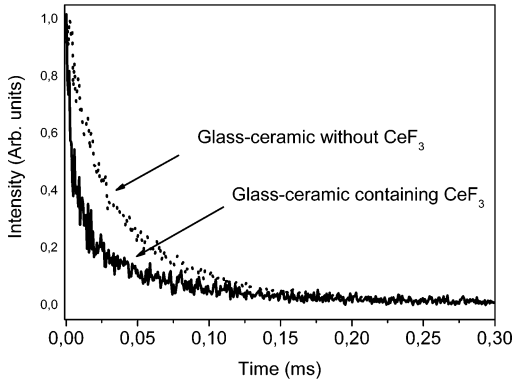

Figure 10. Fluorescence decay curves of the $^4S_{3/2}$ level of Er^{3+} emitting at 540 μm, excited through the $^2H_{11/2}$ level ($\lambda_{excitation} = 519$ nm), for GPF + $0.5ErF_3$ + $1YbF_3$ glass−ceramic (dotted line) and for GPF + $0.5ErF_3$ + $1YbF_3$ + $0.5CeF_3$ glass−ceramic (solid line).

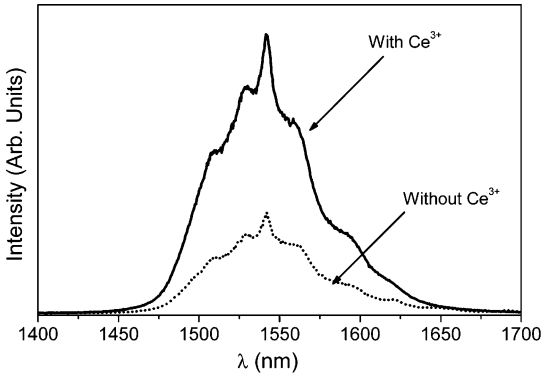

Figure 11. Emission spectra of GPF + $0.5ErF_3$ + $1YbF_3$ glass−ceramic (dotted line) and GPF + $0.5ErF_3$ + $1YbF_3$ + $0.5CeF_3$ glass−ceramic (solid line) ($\lambda_{excitation} = 975$ nm).

measured at 2.7 μm under direct excitation (previously mentioned) is almost 1.6 times longer than the rise time of the $^4I_{13/2}$ level. This may be due to microscopic radiative trapping of the 2.7-μm emission occurring inside the nanocrystallites. Indeed, the high local concentration of Er^{3+} ions embedded inside the crystallites and the long lifetime of the $^4I_{13/2}$ level should promote efficient radiation trapping of the 2.7-μm photons, lengthening artificially the measured $^4I_{11/2}$ level lifetime.

At the opposite, in the glass−ceramic with CeF_3, no rise time is observed (Figure 9b). The $^4I_{13/2}$ level is populated instantaneously after the excitation, confirming that the $^4I_{11/2}$ level has now a very short lifetime. This reflects that, in the presence of CeF_3, the $^4I_{11/2}$ level de-excitation mainly occurs via nonradiative processes and explains the impossibility to measure directly the $^4I_{11/2}$ lifetime, as previously mentioned.

At long time, the two curves are almost parallel (Figure 9a) and the $^4I_{13/2}$ lifetimes are identical to those measured under direct excitation into the $^4I_{13/2}$ level previously mentioned. One can notice the nonexponential character of the decay curve of the CeF_3-containing glass−ceramic at short time (Figure 9b). This behavior can be correlated[3] to the interactions between Er^{3+} ions excited in the $^4I_{13/2}$ level. This phenomenon is not observed in the glass−ceramic without CeF_3, probably because the $^4I_{13/2}$ level is slowly populated, thus limiting the concentration of excited Er^{3+} and preventing energy transfer between excited Er^{3+} ions.

Hence, the addition of CeF_3 shortens the $^4I_{11/2}$ level lifetime to zero but does not affect the $^4I_{13/2}$ level lifetime.

3. Fluorescence Decay Curves of the $^4S_{3/2}$ Level of Er^{3+}. The decrease of the $^4I_{11/2}$ level lifetime in the presence of CeF_3 can explain the strong reduction of the green up-conversion emission (Figure 7). Nonetheless, the 520- and 540-nm bands are reduced by a factor 300 while the emission at 400 nm completely vanishes. To understand the total disappearance of the 400-nm up-conversion emission, the $^4S_{3/2}$ level fluorescence lifetime was measured in glass−ceramics with and without CeF_3.

The fluorescence decay curves of the Er^{3+} $^4S_{3/2}$ level of GPF + $0.5ErF_3$ + $1YbF_3$ and GPF + $0.5ErF_3$ + $1YbF_3$ + $0.5CeF_3$ glass−ceramics were recorded by exciting at 519 nm (Figure 10). The $^4S_{3/2}$ level lifetime was measured in both cases at 540 nm. Due to the nonexponential character of the fluorescence decay curves, an average lifetime $<\tau>$ was determined by integrating the decay curves using the formula: $\int_{t=0}^{t=\infty} I(t).dt = \langle\tau\rangle\, I_{(t\,=\,0)}$. The $^4S_{3/2}$ level average lifetime was evaluated to be 45 ± 5 μs in the glass−ceramic without Ce^{3+} ions and 24 ± 5 μs in the glass−ceramic containing Ce^{3+} ions. Introducing Ce^{3+} ions shortens the $^4S_{3/2}$ level lifetime, indicating that Ce^{3+} ions induce nonradiative de-excitations between the $^4S_{3/2}$ and $^4F_{9/2}$ levels of Er^{3+}.

Like the $^4I_{11/2}$ level, the $^4S_{3/2}$ level lifetime is shortened when CeF_3. As the three-photon up-conversion process implies both the $^4I_{11/2}$ and $^4S_{3/2}$ levels,[16] the decrease of these two levels lifetimes strongly reduces the three-phonon up-conversion process. This is well correlated with the disappearance of up-conversion emission at 400 nm (Figure 7).

4. Energy Transfer Between Lanthanide Ions in Glass−Ceramics. In the Yb:Er-glass−ceramics, three up-conversion mechanisms,[14] populating highly excited levels of Er^{3+}, can occur: the energy transfer up-conversion between Yb^{3+} and Er^{3+} ions, the excited-state absorption from the $^4I_{11/2}$ level of Er^{3+}, and cross-relaxation between Er^{3+} ions such as ($^4I_{11/2}$, $^4I_{11/2}$) → ($^4S_{3/2}$, $^4I_{15/2}$). Further experiments using glass−ceramics with various concentrations in ErF_3 and YbF_3 are needed to distinguish between these mechanisms.

In glass−ceramics containing CeF_3, we proved that the introduction of Ce^{3+} induces new nonradiative de-excitations of the $^4I_{11/2}$ and $^4S_{3/2}$ Er^{3+} levels, indicating that strong interactions exist between Er^{3+} and Ce^{3+}. The energy gap between $^2F_{7/2}$ and $^2F_{5/2}$ of Ce^{3+} (about 2300 cm^{-1} [17]) could enable a cross-relaxation process between the $^4I_{11/2}$ and $^4I_{13/2}$ levels (3200 cm^{-1} at the minimum) and between the $^4S_{3/2}$ and $^4F_{9/2}$ levels (2900 cm^{-1} at the minimum). According to the Ce/Er relative concentration, the most probable cross-relaxation process can occur with phonon assistance between one Er^{3+} and one Ce^{3+} ions. Such Ce−Er interactions were also evidenced in glasses[10] and in $Ca_2Al_2SiO_7$ crystal.[9]

5. Effect of CeF_3 Doping on the 1.54-μm Fluorescence Intensity. The fluorescence spectra around 1.54 μm of the GPF + $0.5ErF_3$ + $1YbF_3$ glass−ceramic and of a CeF_3-containing glass−ceramic were recorded by exciting at 975 nm. Both glass−ceramics were studied in the same conditions, enabling a comparison of the emission intensities.

(17) Elias, L. R.; Heaps, Wm. S.; Yen, W. M. *Phys. Rev.* **1973**, *8* (11), 4989.

These spectra, reported in Figure 11, appear similar with fluorescence lines occurring at the same wavelength in the two samples. The only difference is that the CeF_3-containing glass−ceramic presents an emission at 1.54 μm about 3 times higher than that of the glass−ceramic without CeF_3. This evidences that the cross-relaxation occurring between Er^{3+} and Ce^{3+}, which reduces the up-conversion emission, is at the benefit of the 1.54-μm fluorescence.

Conclusion

Transparent oxyfluoride glass−ceramics doped with ErF_3, YbF_3, and CeF_3 were prepared. Through the synthesis of these tri-doped glass−ceramics, we evidenced the high nucleating character of CeF_3 and a high segregation of the three rare-earth ions into the crystallites with the formation of a solid solution $Pb_{1-x-y-z}Er_xYb_yCe_zF_{2+x+y+z}$.

The addition of cerium fluoride shortened the $^4I_{11/2}$ and $^4S_{3/2}$ lifetimes of Er^{3+} and dramatically decreased the Er^{3+} up-conversion emission. It reveals strong interactions between Er^{3+} and Ce^{3+} ions resulting in a cross-relaxation process. Introducing CeF_3 in glass−ceramics reinforces the 1.54-μm fluorescence, which constitutes a major improvement of these materials. Hence, the synthesis of glass−ceramics tri-doped with ErF_3, YbF_3, and CeF_3 is very promising for future optical applications around 1.54 μm.

CM047821D